Inorganic Chemistry

Article

pubs.acs.org/IC

Lanthanide(III) Complexes of Rhodamine–DO3A Conjugates as Agents for Dual-Modal Imaging

Charlotte Rivas,[†] Graeme J. Stasiuk,[†] Juan Gallo,[†] Florencia Minuzzi,[‡] Guy A. Rutter,[‡] and Nicholas J. Long*[,†]

[†]Department of Chemistry, Imperial College London, South Kensington, London SW7 2AZ, U.K.

[‡]Section of Cell Biology, Division of Diabetes, Endocrinology and Metabolism, Department of Medicine, Imperial College London, South Kensington, London SW7 2AZ, U.K.

Supporting Information

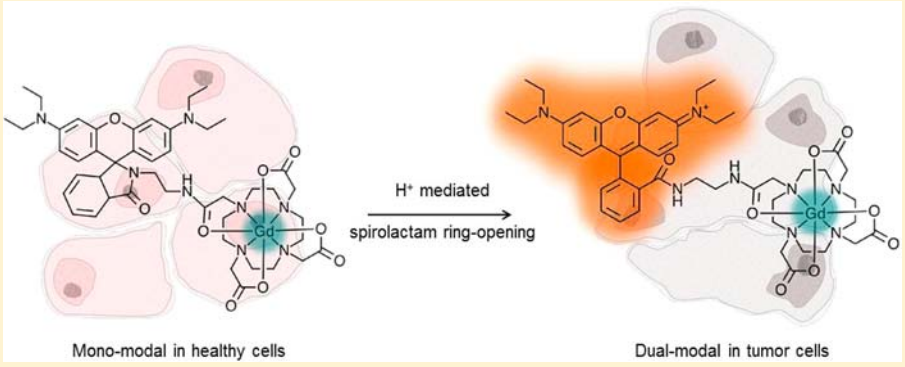

ABSTRACT: Two novel dual-modal MRI/optical probes based on a rhodamine–DO3A conjugate have been prepared. The bis(aqua)gadolinium(III) complex **Gd.L1** and mono(aqua)gadolinium(III) complex **Gd.L2** behave as dual-modal imaging probes (r_1 = 8.5 and 3.8 mM^{-1} s^{-1} for **Gd.L1** and **Gd.L2**, respectively; λ_{ex} = 560 nm and λ_{em} = 580 nm for both complexes). The rhodamine fragment is pH-sensitive, and upon lowering of the pH, an increase in fluorescence intensity is observed as the spirolactam ring opens to give the highly fluorescent form of the molecule. The ligands are bimodal when coordinated to Tb(III) ions, inducing fluorescence from both the lanthanide center and the rhodamine fluorophore, on two independent time frames. Confocal imaging experiments were carried out to establish the localization of **Gd.L2** in HEK293 cells and primary mouse islet cells (~70% insulin-containing β cells). Colocalization with MitoTracker Green demonstrated **Gd.L2**'s ability to distinguish between tumor and healthy cells, with compartmentalization believed to be in the mitochondria. **Gd.L2** was also evaluated as an MRI probe for imaging of tumors in BALB/c nude mice bearing M21 xenografts. A 36.5% decrease in T_1 within the tumor was observed 30 min post injection, showing that **Gd.L2** is preferentially up taken in the tumor. **Gd.L2** is the first small-molecule MR/fluorescent dual-modal imaging agent to display an off–on pH switch upon its preferential uptake within the more acidic microenvironment of tumor cells.

INTRODUCTION

Molecular imaging is a rapidly growing area of chemistry that aims to visualize cellular function and structure in a noninvasive manner with the in vivo use of specially designed imaging agents. The combination of magnetic resonance imaging (MRI) and optical imaging offers synergistic advantages over either modality alone. MRI has high spatial resolution and good soft-tissue contrast[1,2] while optical imaging displays high sensitivity and can give information on the local chemical environment.[3] Lanthanide-based optical probes have superior fluorescence properties in comparison to organic fluorophores, with luminescence lifetimes stretching to the millisecond region, and time-gated techniques can be employed in order to eliminate interfering background autofluorescence.[4−6]

With the constant advances in cancer treatment, it is becoming increasingly important to detect the early signs of the disease and to establish the efficacy of the concurrent treatment in a noninvasive manner. This can be achieved by the in vivo use of a dual-modal MRI/fluorescent probe that responds to a characteristic trait of tumor cells.[7−9] It is known that the mitochondrial potential in cancer cells is greater than that of healthy cells,[10] and the design of a probe that can accumulate in these energized mitochondria will lead to a tumor-targeting agent. The combination of MRI and fluorescence will allow for improved diagnostic accuracy by tumor localization via MRI imaging and guided surgery via fluorescence imaging.

MRI is a noninvasive diagnostic technique that relies on the enhancement of local water proton relaxation.[11,12] Different tissues have different relaxation times, resulting in endogenous

Received: September 2, 2013
Published: December 4, 2013

Scheme 1. Synthesis of L1 and Ln.L1 (Ln = Gd, Tb)[a]

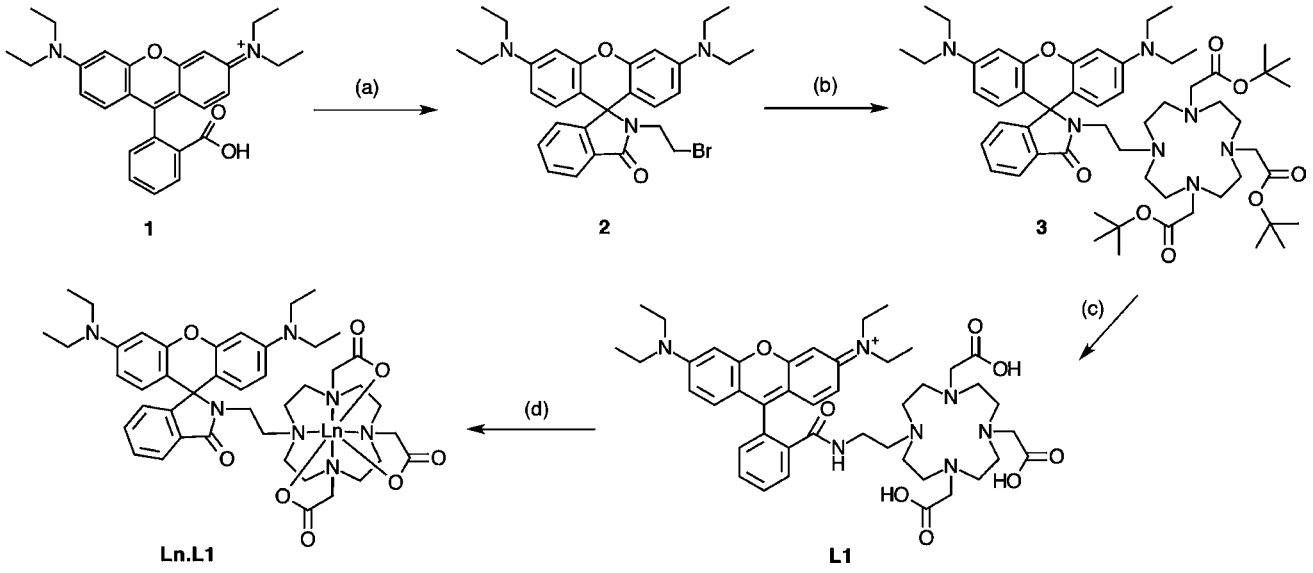

[a]Reagents and conditions: (a) (i) $POCl_3$, reflux, 18 h; (ii) bromoethylamine, CH_3CN, room temperature, 24 h. (b) Tri-*t*-Bu-DO3A, K_2CO_3, CH_3CN, reflux, 24 h. (c) TFA, DCM, room temperature, 16 h. (d) $LnCl_3{\cdot}6H_2O$, H_2O, NaOH(aq), pH 5.5, room temperature, 24 h.

magnetic resonance contrast. Exogenous agents can be used to enhance this contrast by selectively shortening the T_1 (longitudinal) or T_2 (transverse) relaxation time; these agents include Gd(III) chelates, manganese complexes, and superparamagnetic nanoparticles.[13,14] The most successful and commonly used of these exogenous agents are complexes containing the Gd(III) ion because of its high magnetic moment ($7.9\mu_B$) given by its seven unpaired electrons and its totally symmetric electronic ground state ($^8S_{7/2}$).[15] According to Solomon−Bloembergen−Morgan theory, the relaxivity of Gd(III) complexes is governed by a number of factors, including the number of bound water molecules (q), the rotational tumbling time (rotational correlation time) of the complex (τ_R), and the mean residence lifetime of Gd(III)-bound water molecules (τ_M).[2] An effective way to increase the relaxivity of a Gd(III) complex is to increase the number of bound water molecules. Herein we report two novel probes possessing different hydration states. We envisioned that the relaxivity could be improved by decreasing the number of coordination sites on the Gd(III) chelate from eight to seven, allowing for a change from one bound water molecule to two. It is reported however that heptadentate ligands, when bound to Gd(III), have unfavorable properties for use as MRI probes in terms of thermodynamic and kinetic stability because of the coordinatively unsaturated nature of the complex.[16]

Eu(III) and Tb(III) chelates based on a DO3A core have received a lot of interest as luminescent lanthanide systems.[17−20] These lanthanides are characterized by their long-lived luminescent excited states (ms time scale) and linelike emission spectra, and their complexes have been shown to be useful in biomedicine as luminescent probes.[21] Lanthanide metals or ions however, have low absorption coefficients due to Laporte-forbidden f−f transitions.[22] This can be overcome by attaching an aromatic chromophore to the macrocyclic core to act as an "antenna" by transferring absorbed excitation energy from its triplet excited state to the excited state of the coordinated lanthanide ion.[23] Rhodamine derivatives have received significant attention as fluorescent labeling agents because of their long absorption and emission wavelengths, large absorption coefficients, and high quantum yields.[24] They have been used in a wide range of applications, having great success as chemosensors (both in vitro and in vivo),[25,26] protein labels,[27] and dual-modal imaging agents.[28,29] Rhodamine derivatives have had particular success as mitochondria targets,[30−32] as their delocalized organic cationic forms tend to accumulate in the mitochondria of tumor cells as a result of the increased negative mitochondrial potential.[33−35] The spiro ring-opening mechanism of rhodamine has also led to its extensive use as a chemosensor for metal detection as well as a pH-sensitive probe.[36−38] Under acidic conditions, the rhodamine moiety exists in its highly fluorescent pink-colored open form. Upon addition of OH^-, the structure exists in its spirocyclic form, which is colorless and nonfluorescent.

In recent years there have been an increasing number of reports of multimodal imaging probes wherein two or more imaging modalities are combined.[39,40] The combination of modalities leads to probes that give enhanced visualization and improved reliability of data by synergistically combining imaging techniques to overcome their inherent disadvantages. MRI gives high anatomical resolution and deep tissue penetration but lacks sensitivity. Optical imaging, however, boasts high sensitivity but has limited tissue penetration. As discussed earlier, the combination of the two techniques yields a probe that is able to provide a more complete picture of the biological area of interest. There are few reports of dual-modal MRI/optical imaging agents in the literature that are not of nanoparticle nature. These include Gou et al.'s description of the binding of a cyanine−DTPA conjugate to BSA to afford relaxivity rate constants of 15 mM^{-1} s^{-1}.[41] The aliphatic nature of the chelate is unfavorable, however, as release of Gd(III) ions into the body from these types of complexes has been related to nephrogenic systemic fibrosis (NSF).[42] In 1998, it was reported that a rhodamine−Gd(III) complex conjugate showed no MRI contrast enhancement when introduced to *Xenopus laevis* embryos.[43] The same complex conjugate, Gd(Rhoda-DOTA), was studied alongside a series of hydrophobic fluorescent dye−Gd(III) complex conjugates in 2011 by Yamane et al.,[44] who found that incorporation of the hydrophobic fluorescent moiety

dx.doi.org/10.1021/ic402233g | *Inorg. Chem.* 2013, 52, 14284−14293

Scheme 2. Synthesis of L2 and Ln.L2 (Ln = Gd, Tb)[a]

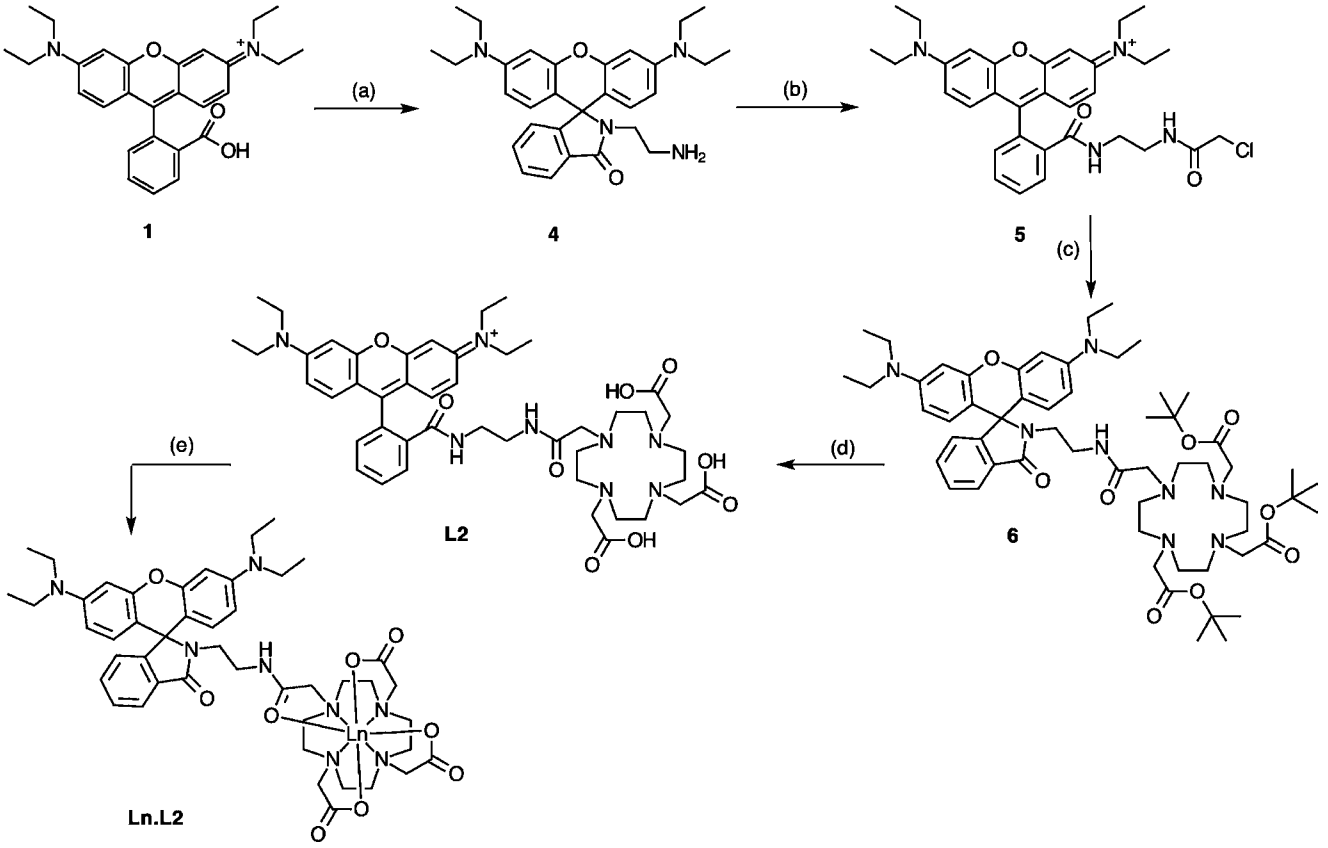

[a]Reagents and conditions: (a) Ethylenediamine, EtOH, reflux, 24 h. (b) Chloroacetyl chloride, NEt_3, DCM, room temperature, 2 h. (c) Tri-*t*-Bu-DO3A, K_2CO_3, CH_3CN, reflux, 24 h. (d) TFA, DCM, room temperature, 16 h. (e) $LnCl_3{\cdot}6H_2O$, H_2O, NaOH(aq), pH 5.5, room temperature, 24 h.

improves cell permeability compared to Gd(DOTA). They reported that Gd(Rhoda-DOTA) showed a large increase in r_1 relaxivity when bound to albumin and efficient cell permeation when incubated with HeLa cells. Again, however, no significant change in the MR signal of HeLa cells was observed in the presence of the complex, even though its fluorescence was observed by microscopy. Similarly, a rhodamine moiety has previously been conjugated to DO3A and consequently labeled with ^{64}Cu to arrive at a dual-modal PET/optical probe.[29] It was found that ^{64}Cu(DOTA-LRB) had a surprisingly high tumor uptake compared with other ^{64}Cu-labeled organic cations. The probe was able to selectively localize to the tumor mitochondria with long tumor retention times.[45] The probe and its derivatives have been the subjects of extensive in vitro and in vivo studies showing that there is promise for a Gd(III) MRI/optical analogue to be as successful in vivo.

In this paper, we report two novel methods for conjugating fluorescent rhodamine derivatives to DO3A. We evaluated the two rhodamine−DO3A Gd(III) derivatives as multimodal MRI/optical imaging agents by measuring their relaxivity and fluorescence properties as well as their in vitro tumor cellular localization. The Tb(III) analogues were synthesized to assess their dual-luminescence properties, and it was found that the organic and metal-based luminescence can be separated on different time scales.

RESULTS AND DISCUSSION

Synthesis. Two new synthetic routes were developed to obtain **L1** and **L2** (outlined in Schemes 1 and 2, respectively), both commencing from commercially available rhodamine B and involving five straightforward steps. Reaction of the carboxylic acid moiety on rhodamine B with bromoethylamine resulted in amide bond formation, giving product **2**. The ligand precursor **3** was prepared by N-alkylation of the tri-*tert*-butyl ester derivative of cyclen (tri-*t*-Bu-DO3A). Removal of the *tert*-butyl ester groups was then carried out using trifluoroacetic acid (TFA) to obtain **L1**. The successful isolation of the product was confirmed through ^{1}H and ^{13}C NMR spectroscopy along with high-resolution mass spectrometry. **L1** was coordinated to a series of lanthanide metal chloride salts [Ln = Gd(III), Tb(III)] in water in a mildly acidic environment (pH ∼5.5). After purification, the absence of free lanthanide ions was verified by the use of xylenol orange indicator solution.[46] For each complex, a peak corresponding to the molecular ion with the correct isotopic pattern could be observed by high-resolution electrospray ionization mass spectrometry. The **Ln.L1** complexes were found to be only partially water-soluble and therefore unsuitable for in vivo applications. Thus, the second ligand **L2** was developed to overcome the solubility issues of **L1** in water. The synthesis of **L2** was very similar to that of **L1**. Two subsequent amide bond formation reactions on rhodamine B were carried out, first with ethylenediamine to form **4** and then with chloroacetyl chloride resulting in product **5**. This was then conjugated to tri-*t*-Bu-DO3A to give **6** in 39% yield, and subsequent deprotection with TFA gave **L2** in the same manner as for **L1**. The second amide bond was introduced to increase the hydrogen-bond donor and acceptor ability and thereby to increase the water solubility. **L2** was

dx.doi.org/10.1021/ic402233g | Inorg. Chem. 2013, 52, 14284−14293

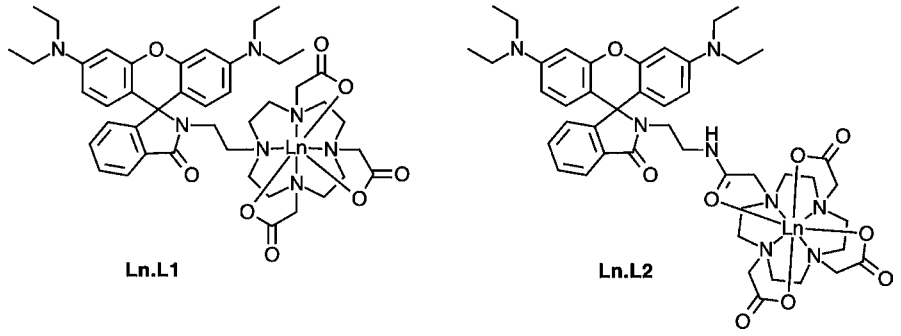

Figure 1. Structures of **Ln.L1** and **Ln.L2** [Ln = Gd(III), Tb(III)].

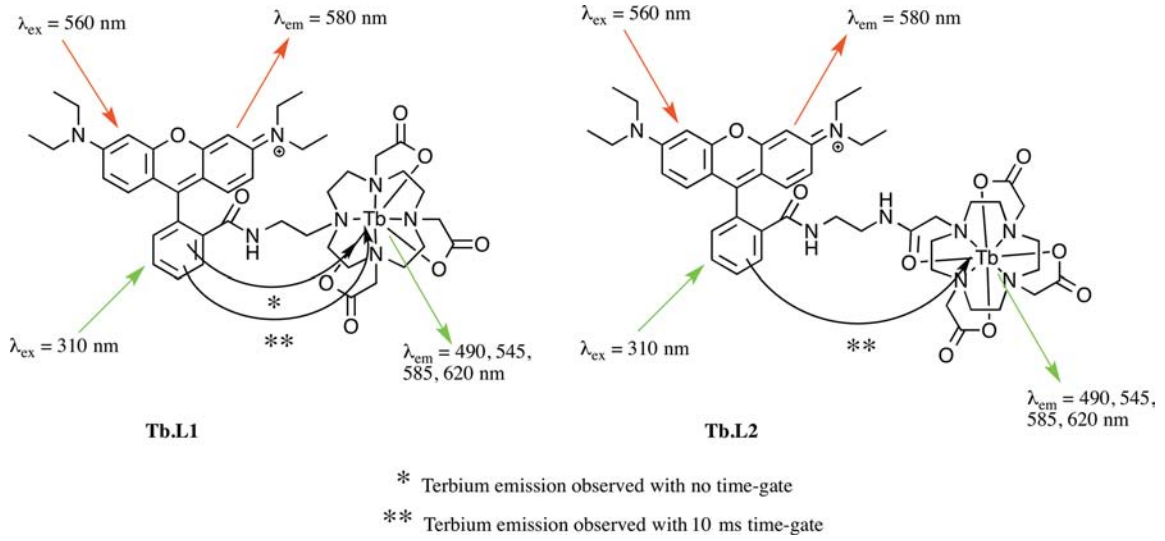

Figure 2. Fluorescence emission pathways in **Tb.L1** and **Tb.L2**.

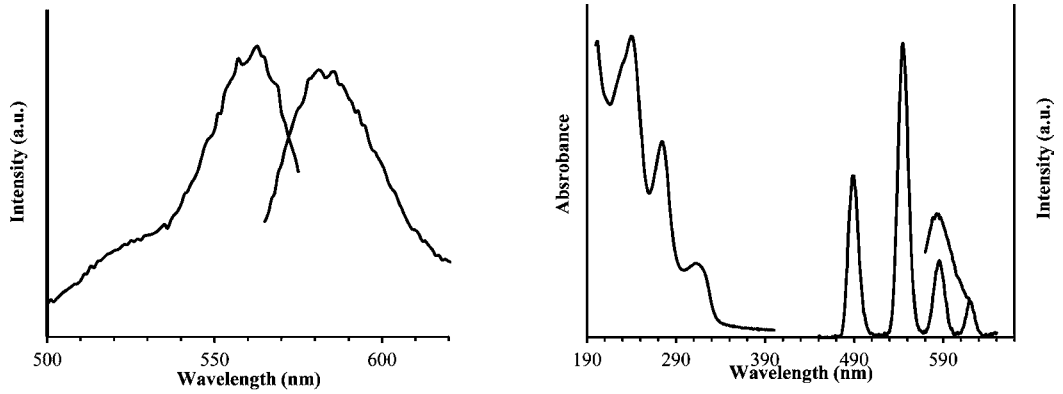

Figure 3. Left panel: excitation spectrum (left) and emission spectrum (right) of **Gd.L2** with λ_{em} = 580 nm and λ_{ex} = 560 nm (0 ms delay). These are also representative spectra of **Gd.L1**. Right panel: absorption spectrum (left), terbium emission (center), and rhodamine fluorescence (right) of **Tb.L2** with λ_{em} = 545 nm and λ_{ex} = 310 and 560 nm, respectively (0.1 ms delay for terbium emission). These are also representative spectra of **Tb.L1**, although no delay was needed to observe the terbium emission. All of the **Ln.L1** complex measurements were carried out in methanol, and all of the **Ln.L2** complex measurements were carried out in H_2O (pH 7.4, 298 K, 100 μM concentration).

complexed with Gd(III) and Tb(III) as above, and the complexes **Ln.L2** were found to be water-soluble.

Photophysical Properties. Complexes **Ln.L1** and **Ln.L2** (Figure 1) behave as dual-modal MRI/optical imaging probes with Gd(III) and dual-luminescent probes with Tb(III). In this section, we discuss the photophysical properties of both systems. The photophysics of the two ligands with Gd(III) were found to be very similar, as they exhibited fluorescence emission at 580 nm upon excitation at 560 nm. This short Stokes shift and orange fluorescence was expected, as the fluorescence properties of rhodamine and its derivatives have been extensively studied.[47] Modification of the carboxylic acid moiety of rhodamine B does not lead to significant changes in the photophysical properties of the chromophore, as no

dx.doi.org/10.1021/ic402233g | Inorg. Chem. 2013, 52, 14284−14293

electronic or structural changes occur on the xanthene core, so a very small bathochromic shift is observed (rhodamine B: λ_{ex} = 553 nm, λ_{em} = 572 nm in ethanol).

The photophysical properties of the Tb(III) analogues were investigated (Figure 2). Under excitation at λ_{ex} = 310 nm, complex **Tb.L1** displays exclusively green emission arising from $^5D_4-^7F_J$ transitions of terbium. The rhodamine-centered emission is of a very low intensity in comparison with the Tb(III) emission, indicating efficient ligand-to-lanthanide energy transfer. At λ_{ex} = 560 nm, emission is seen at 580 nm, featuring fluorescence from the xanthene core. Therefore, two fluorescence pathways are available to **Tb.L1**: emission via the lanthanide with energy transfer from rhodamine and direct excitation of the xanthene core. Conversely, under excitation at λ_{ex} = 310 nm, the emission spectrum of complex **Tb.L2** is dominated by rhodamine emission at 580 nm. Applying a 0.1 ms delay to the fluorescence measurement allowed for isolation of the short-lived organic fluorescence of the rhodamine moiety from the long-lived lanthanide luminescence in both complexes. The extra amide bond in **L2** renders the complex water-soluble but also introduces a quenching pathway. The additional N−H bond is close to the lanthanide center, and fluorescence deactivation may occur via the N−H vibrational energy level oscillator.[48]

Therefore, when complexed with a luminescent lanthanide ion, both ligands behave as dual-luminescent probes. In both **Tb.L1** and **Tb.L2**, excitation at 560 nm leads to emission from the organic chromophore at 580 nm, with the fluorescence originating from the xanthene core. Using time-gating techniques, Tb(III) emission is induced in both complexes upon excitation of the isolated phenyl ring of the rhodamine moiety at 310 nm by energy transfer to the Tb(III) metal center (Figures 2 and 3). In **Tb.L1** only, Tb(III) emission can be seen upon excititation at 310 nm without the use of a time delay. The quantum yields of both terbium complexes were determined, and the results were in agreement with the observed spectra, confirming the efficient energy transfer to the terbium metal center in **Tb.L1** (Φ = 18.6%) and the inefficient energy transfer in **Tb.L2** (Φ = 0.8%).

The luminescence decays of the Tb(III) complexes in both H_2O and D_2O were also measured (see the Supporting Information). The luminescence lifetimes in D_2O were increased in comparison to H_2O because less nonradiative deactivation was induced by O−D vibrations than by O−H vibrations.[49] From these differences in the rates of energy transfer to H_2O and D_2O oscillators, the hydration state can be calculated using eq 1, in which the term 0.06 reflects the

$$q_{Tb} = 5(\Delta k - 0.06 - 0.01n) \quad (1)$$

quenching effect of unbound water molecules and n is the number of coordinated secondary amide groups, reflecting the quenching effect of the proximate NH oscillators.[50] The emission decays were fitted to monoexponential decays, and the corresponding lifetime measurements of both terbium complexes confirmed the expected coordination numbers of seven for **Tb.L1** and eight for **Tb.L2** (Table 1).

Relaxometric Studies. T_1 measurements of the Gd(III) complexes were performed at 400 MHz (9.4 T, 25 °C), and their r_1 values were determined. The r_1 values of 8.5 and 3.8 mM^{-1} s^{-1} obtained for complexes **Gd.L1** and **Gd.L2**, respectively, were within the range for Gd(III) chelates with hydration states of two and one respectively. These hydration states were confirmed by the lifetime measurements of the terbium analogues.

Table 1. Selected Photophysical Data for Complexes Tb.L1 and Tb.L2

complex	τ_{H_2O}/ms	τ_{D_2O}/ms	q	ϕ_{em}/%
Tb.L1	1.23	2.53	1.8	18.6
Tb.L2	1.55	2.05	0.8	0.8

It is well-known that the presence of hydrophobic moieties within a probe is one of the basic structural requirements for ligand binding to human serum albumin (HSA).[51] HSA is the most abundant protein in blood, and binding to it results in an increase in intravascular retention and relaxivity (due to a decrease in τ_R of the complex).[52] In view of the fact that the rhodamine moiety has extended aromatic rings and hence hydrophobicity, a study was carried out to investigate possible interactions between **Gd.L2** and HSA. The relaxation rates of a series of solutions of **Gd.L2** with increasing concentrations of HSA were measured. The relaxation rate was found to remain constant across the series (Figure 4), therefore indicating that

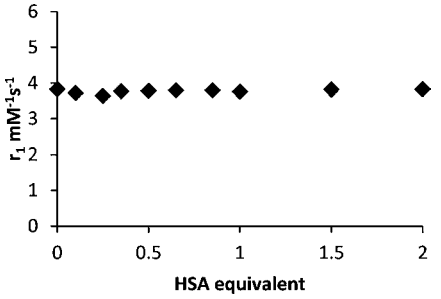

Figure 4. Titration of **Gd.L2** with HSA.

there is no significant binding of the probe to the protein. The binding mechanisms of rhodamine B with bovine serum albumin (BSA) were previously investigated, and site-selective binding was observed. However, these results were obtained using high molar ratios of rhodamine B to BSA (>50).[53] Such high concentrations are not practical for use of MRI probes in vivo, and indeed, large changes in relaxivity have been observed in cases where the molar ratio of probe to serum albumin have been much lower.[54,55] It is hypothesized that the steric bulk of the complex is unsuitable for selective binding to HSA.

pH Titration. As previously discussed (vide supra), the lactam ring of rhodamine can be intramolecularly opened and closed via changes in pH.[36] The pH sensitivity of **Gd.L2** was investigated, and to show the sensitivity of the proton-triggered ring opening, a pH titration was carried out wherein the emission intensity was monitored at various pH values (Figure 5). The pH titration showed that **Gd.L2**, which was nonfluorescent at pH 6.5 or above, rearranged into its fluorescent form at acidic pH. The fluorescence of **Gd.L2** at pH 4.3 was 50-fold brighter than that at pH 6.5 and 15-fold brighter than that at pH 6.0, demonstrating that **Gd.L2** is a sensitive, acid-responsive probe capable of sensing small changes in pH in the range 4−7.

A titration curve was produced by plotting the emission intensity at λ_{em} = 580 nm versus pH, which yielded a pK_a value of 5.11. It was hypothesized that the change in the charge of **Gd.L2** on going from pH ∼ 7.0 to 4.0 would aid the probe to

dx.doi.org/10.1021/ic402233g | Inorg. Chem. 2013, 52, 14284−14293

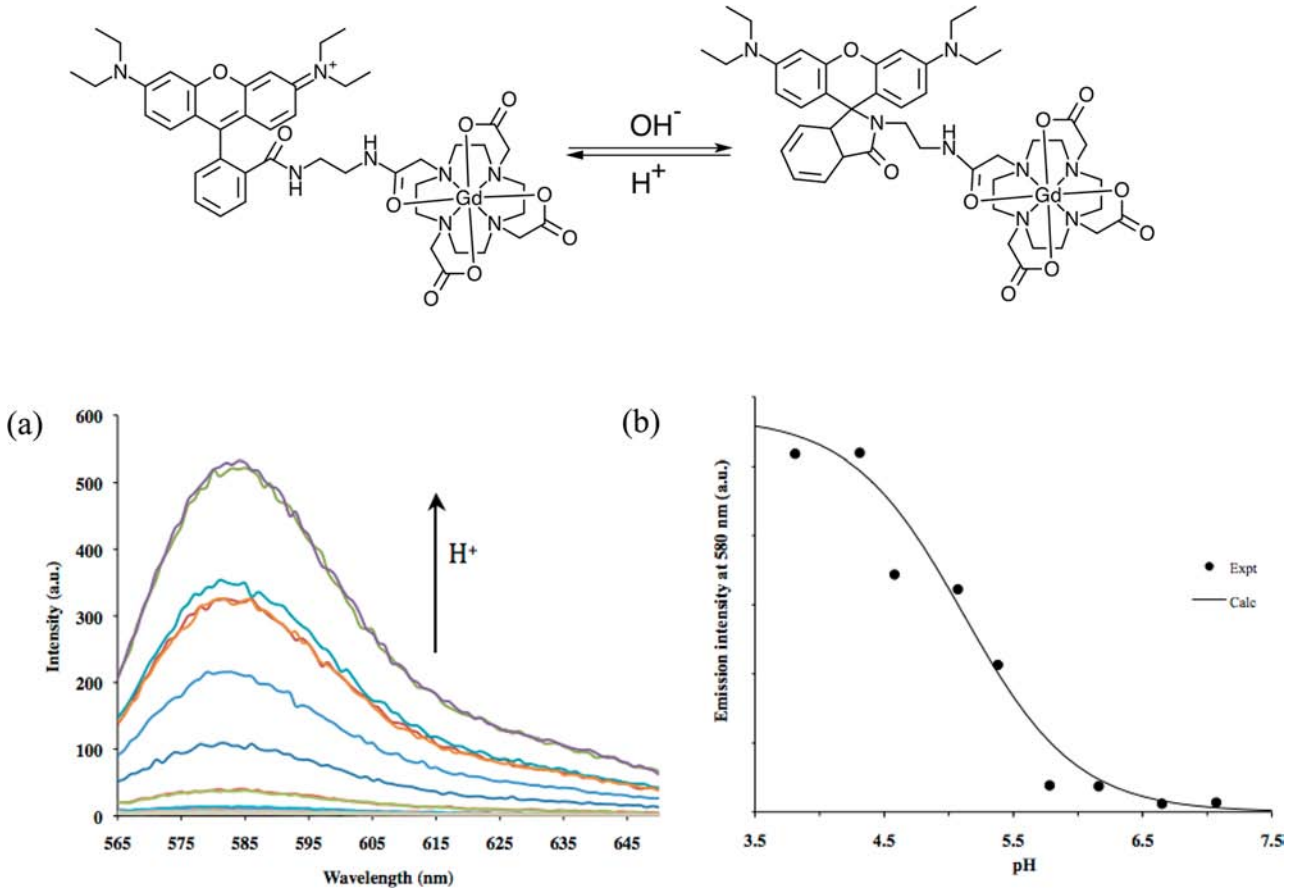

Figure 5. Upper panel: pH-mediated ring opening of the intramolecular sprirolactam of **Gd.L2**, yielding a highly fluorescent species. Lower panels: (a) pH-dependent emission spectra of **Gd.L2** (λ_{ex} = 560 nm, λ_{em} = 580 nm); (b) pH titration curve used to determine pK_a.

localize in the more acidic microenvironment of tumor cells.[56] It has been shown that the microenvironment of tumor cells is more acidic than that of healthy tissues (Warburg effect). Upon entering an acidic environment, the probe can undergo rearrangement to its ring-opened form, which is fluorescent. This cationic acid form of the probe would then be expected to accumulate in the mitochondria.[57]

In Vitro/in Vivo Studies. To test the viability of **Gd.L2** as a dual-modal agent for cancer imaging, in vivo and in vitro studies were carried out. Because of a lack of water solubility, no in vivo studies could be carried out on **L1** complexes. The addition of an extra amide functionality within **L2** introduced water solubility, and this allowed for the investigation of its biological properties via in vitro and in vivo studies. Cell penetration is crucial for the use of imaging probes in the monitoring of biological mechanisms. To this end, preliminary in vitro cell studies were carried out using **Gd.L2**. Rhodamine has been widely used to determine the mitochondrial potential in tumor cells.[9] The negative mitochondrial potential is reported to be greater in tumor cells than in normal cells, and organic cations such as rhodamine have been shown to accumulate in the energized mitochondria.[57,58] With this in mind, colocalization experiments were undertaken wherein a known mitochondrial stain (MitoTracker Green FM) was tested against **Gd.L2**. Confocal microscopy images of human embryonic kidney (HEK293) cells and primary mouse islet cells (~70% insulin-containing β cells) were recorded after a 30 min incubation with **Gd.L2** and MitoTracker Green (Figure 6).

Images B, C and E, F in Figure 6 show clear accumulation of **Gd.L2** within each cell type. However, a clear colocalization of **Gd.L2** and MitoTracker was not evident (Figure 6C, box). Moreover, we noted that in cells where significant uptake of **Gd.L2** was apparent (as indicated in the primary cells in D–F), MitoTracker accumulation was lower and more diffuse than in neighboring cells, and little, if any, colocalization of red and green staining was evident (Figure 6F). These findings are probably best explained by the fact that the **Gd.L2** fluorescence, which is strongly suppressed at pH >6.5 (Figure 5B), is only readily detectable in cells in which mitochondria are relatively depolarized, such that the mitochondrial matrix pH falls to levels permissive of **Gd.L2** fluorescence. Such mitochondria, however, are expected to be poorly able to retain MitoTracker, whose accumulation depends on the inner mitochondrial membrane potential and the pH gradient (i.e., high intramitochondrial pH >7). These results are thus consistent with the known properties of both MitoTracker and **Gd.L2** but are unable to definitively establish a mitochondrial localization of the latter.

BALB/c nude mice with neck M21 (human melanoma cell) xenograft implantations were injected intravenously with 0.1 mmol kg^{-1} **Gd.L2**. The mice were imaged in a 4.7 T MRI instrument at different times (preinjection, 30 min post injection, and 60 min post injection) to evaluate the effect of the contrast agent. Thirty minutes after the injection of **Gd.L2**, a 36.5% decrease in tumor average T_1 was observed compared with the baseline of the preinjection image (Figure 7a,b). This decrease in longitudinal relaxation time was retained at least up

dx.doi.org/10.1021/ic402233g | Inorg. Chem. 2013, 52, 14284–14293

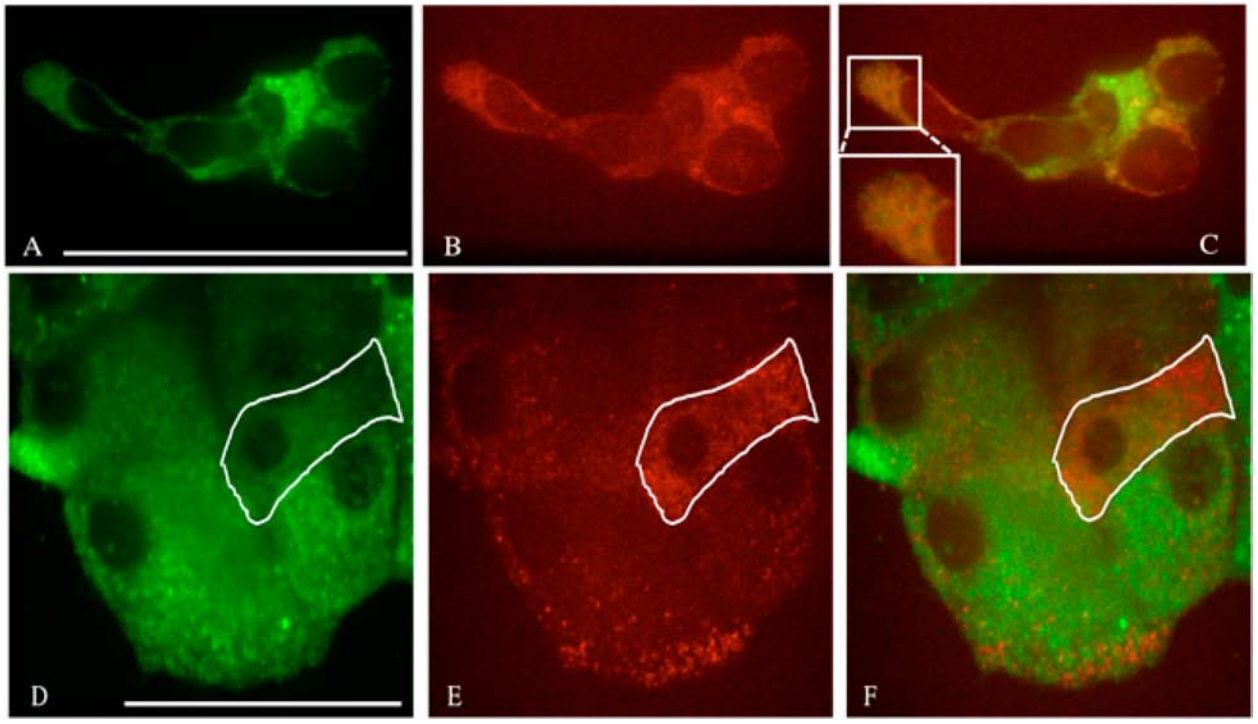

Figure 6. (A–C) Confocal microscopy images of HEK cells. Cells were incubated with 215 mM **Gd.L2** and 100 nM MitoTracker Green for 30 min, washed twice with KREBS buffer, and visualized under a fluorescence microscope. (A) MitoTracker Green signal. (B) **Gd.L2** signal. (C) Merged signals. Scale bar: 50 μm. (D–F) Confocal microscopy images of dissociated primary mouse islet cells. Cells were incubated with 215 mM **Gd.L2** and 100 nM MitoTracker Green for 30 min, washed twice with KREBS buffer, and visualized under a fluorescence microscope. (D) MitoTracker Green signal. (E) **Gd.L2** signal. (F) Merged signals. Scale bar: 50 μm.

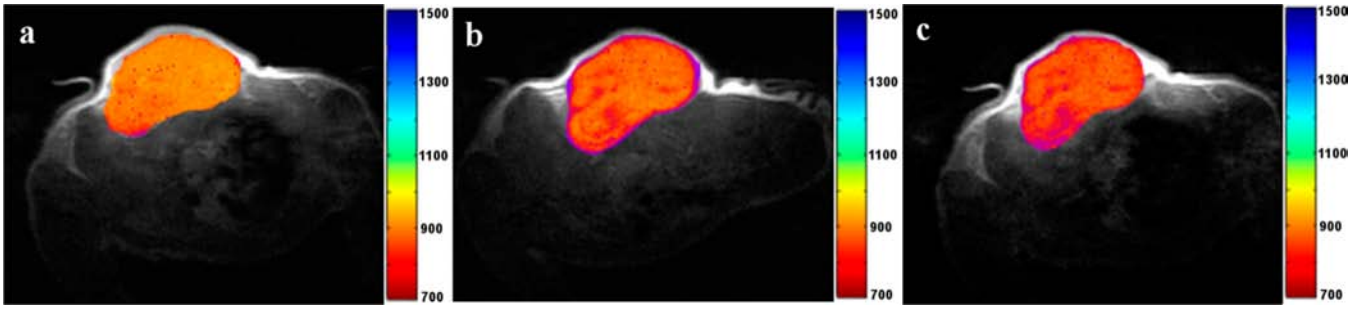

Figure 7. Parametric T_1 maps of a BALB/c nude mouse tumor: (a) preinjection; (b) 30 min post injection with **Gd.L2**; (c) 60 min post injection with **Gd.L2**. Scale bars in ms.

to 60 min (31.3% decrease; Figure 7c). These preliminary images demonstrate that **Gd.L2** functions successfully in vivo by shortening the T_1 of protons in the tumor sufficiently so as to give a more detailed image. The observed accumulation of **Gd.L2** in the tumor area is consistent with the predicted effect of a lower pH environment on the probe; the rearrangement of the lactam ring at acidic pH introduces a positive charge in the molecule that can promote the intracellular uptake of the molecule responsible of the average T_1 decrease observed in the tumor.

CONCLUSIONS

We have reported the preparation and full characterization of two rhodamine–DO3A conjugate derivatives. The DO3A units have been coordinated to paramagnetic Gd(III) and luminescent Tb(III) centers. Complexation with Tb(III) gives dual-luminescent probes with two different time scales, and photophysical data collected also show the impact of distance of the sensitizer and linker design from the lanthanide metal center on the efficiency of energy transfer. When complexed with Gd(III), they form dual-modal MRI/fluorescent probes. **Ln.L2** is water-soluble and suitable for in vitro/in vivo studies, and **Gd.L2** has r_1 = 3.84 mM^{-1} s^{-1} (9.4 T, 25 °C) and has been shown to be viable both in vitro and in vivo. The pH sensitivity of the probe means that it functions as an "off–on" luminescent probe that is sensitive to the small pH changes within cells. By coexpression with a known mitochondrial stain, the probe has been hypothesized to localize in the mitochondria of HEK cells. These studies demonstrate that the probe is cell-penetrating, has a pH sensitivity to acidic microenvironments, and is a tumor specific, dual-modal MRI/fluorescent contrast agent.

EXPERIMENTAL SECTION

Materials and Conditions. No special precautions were taken to exclude air or moisture during reactions or workups, unless otherwise stated. Products **2**[59] and **4**[60] were prepared via literature methods from

commercially available starting materials. All other materials were purchased from commercial suppliers and used without further purification.

Instrumentation. ^{1}H and $^{13}C\{^{1}H\}$ NMR spectra were recorded at ambient temperature on a Bruker 400 MHz spectrometer and internally referenced to the residual solvent peaks of $CDCl_3$ at 7.26 ppm (^{1}H) and 77.16 ppm ($^{13}C\{^{1}H\}$) or MeOD at 3.31 ppm (^{1}H) and 49.15 ppm ($^{13}C\{^{1}H\}$). $^{13}C\{^{1}H\}$ spectra were fully assigned where possible using 2D correlation spectroscopy. Mass spectrometry analyses were conducted by the Mass Spectrometry Service, Imperial College London. Microanalyses were carried out by Stephen Boyer of the Science Centre, London Metropolitan University. ICP-MS analysis was carried out by Stanislav Strekopytov of the Natural History Museum.

Fluorescence Measurements. Absorption and fluorescence spectra of all complexes in either aqueous or methanolic solutions depending on solubility were obtained at room temperature on a PerkinElmer Lambda 25 spectrometer and a Cary Varian luminescence spectrometer (using SCAN for Windows), respectively. Samples were held in 10 mm × 4 mm quartz Hellma cuvettes. Lifetimes were measured by direct excitation of the sample at 325 nm with a 40 ms pulse of light (50 pulses per point) followed by monitoring of the integrated intensity of light emitted at 545 nm during a fixed gate time of 0.1 ms at a delay time later. Delay times were set at 0.1 ms, covering four or more lifetimes. Excitation and emission slits were set to 10:10 nm bandpass respectively. The obtained decay curves were fitted to a simple monoexponential first-order decay curve using Microsoft Excel. Fluoresence quantum yields of terbium complexes were determined from the integrated fluorescence intensities of the complexes following a previously reported method[61] using the reference compound[62] $Na_3[Tb(dpa)_3]$ in water or methanol at 279 nm (quantum yield = 26.5% or 18.2%, respectively).

pH Titration. A 1.49 mM solution of **Gd.L2** in 0.1 M NaCl (1 mL) was prepared, from which 15 × 67 μL aliquots (microlitre pipet, Eppendorf) were taken. Each aliquot was adjusted to the required pH using a digital pH meter (Jenway 3510) equipped with a glass electrode (Jenway 924005). The pH was monitored and adjusted to acidic or basic conditions using small aliquots of a 1 M HCl or 1 M NaOH solution, respectively. The pH was allowed to stabilize. The solution was then added to a quartz cuvette for fluorescence analysis. The fluorimeter was operated using an excitation slit width of 10 nm and an emission slit width of 2.5 nm.

Relaxivity Measurements. **Gd.L1** was dissolved in a methanol/water (50:50) solvent mixture to give a solution of concentration 5 mM. **Gd.L2** was dissolved in water to give a solution concentration of 5 mM. The resulting solutions were placed in 1.7 mm diameter capillaries, which were sealed. The $1/T_1$ measurements were performed on a Bruker Avance 400 spectrometer (400 MHz). These experiments were carried out a minimum of three times, and the relaxivity results given are averages of all experiments. The concentration of Gd(III) was checked by the chemical shift measurement of HOD induced by magnetic susceptibility.[63]

HSA Relaxivity Titration. A 1.49 mM solution of **Gd.L2** in 0.1 M NaCl (pH 7.4) was prepared, from which 10 × 67 μL aliquots were taken. To each aliquot was added an aliquot of a 2 mM solution of HSA (0.1 M NaCl, pH 7.4) to give 10 different sample concentrations (0, 0.1, 0.25, 0.35, 0.5, 0.65, 0.85, 1, 1.5, and 2 equiv of HSA). The solutions were made up to a volume of 100 μL by addition of water where required. The resulting solutions were placed in 1.7 mm diameter capillaries, which were sealed. The $1/T_1$ measurements were performed on a Bruker Avance 400 spectrometer (400 MHz).

In Vivo Tumor Models. All of the animal experiments were performed by licensed investigators in accordance with the United Kingdom Home Office Guidance on the Operation of the Animal (Scientific Procedures) Act 1986 and in keeping with the newly published guidelines for the welfare and use of animals in cancer research.[64] Female BALB/c nude mice (aged 6−8 weeks; Harlan) were used. M21 cells were injected subcutaneously on the back of mice (5×10^6 cells in 100 μL of sterile PBS). Animals were used when the xenografts reached ∼100 mm^3. Tumor dimensions were measured continuously using calipers, and tumor volumes (V) were calculated using the equation $V = \pi abc/6$, where a, b, and c represent the lengths of the three orthogonal axes of the tumor.

In Vivo MRI. In vivo MRI was performed in a 4.7 T horizontal-bore DirectDrive MRI system (Varian, Palo Alto, CA, USA) equipped with 40 G/cm actively shielded gradients (VnmrJ 3.1). For imaging of the tumors and generation of the T_1 parametric maps, a 45 mm diameter saddle coil was used in transmit mode and a separate 20 mm diameter stripline resonator was used as a surface coil to accommodate the tumors.[65] Imaging was performed with an inversion recovery (IR) sequence and the following parameters: axial images; FOV = 35 × 35 mm; No slices = 14; slice thickness = 1 mm (zero slice gap); image bandwidth = 156 kHz; T_R = 4500 ms; T_I = 6, 14.6, 35.4, 86.1, 209, 508, 1230, or 3000 ms; NA = 2; image matrix = 192 × 192; TA = 12 min. During imaging, animals were anesthetized with 2% isofluorane and respiration and body temperature were monitored via SA physiological monitoring systems (SA Instruments, Stony Brook, NY, USA). Body temperature was monitored by a rectal probe and maintained at 35 ± 1 °C. T_1 maps were generated in ImageJ[66] by fitting the acquired data to the equation $S = S_0[1 - 2\exp(-T_I/T_1)]$, where T_I is the inversion time and T_1 is the longitudinal relaxation time. In order to assign the signal with the appropriate sign for the fitting process, the χ^2 value of the fit was evaluated during the fitting. ROIs were then drawn on the T_1 maps to delineate the whole tumor with consideration to avoid the edges of the tumor and thus contamination from neighboring tissues and partial volume effects.

In Vitro Cell Culture and Imaging. HEK293 cells were cultured in DMEM (Lonza) supplemented with 10% fetal bovine serum (FBS) (Lonza), 1% glutamine (Lonza), and 1% penicillin/streptomycin (Gibco). On the day of visualization, cells were washed twice with KREBS buffer (140 mM NaCl, 3.6 mM KCl, 0.5 mM NaH_2PO_4, 0.2 mM $MgSO_4$, 1.5 mM $CaCl_2$, 10 mM HEPES, pH 7.4, 2 mM $NaHCO_3$) pre-equilibrated with 95:5 O_2/CO_2 and containing 25 mM glucose. Cells were then incubated with KREBS buffer containing 215 mM **Gd.L2** and 100 nM MitoTracker Green for 30 min and washed twice with KREBS buffer before visualization. Images were captured using a Zeiss Axiovert confocal microscope coupled to a Nipkow spinning-disk head (Yokogawa CSU-10) using a 63× oil objective. A solid-state laser (CrystaLaser) controlled by a laser-merge module (Spectral Applied Physics) provided wavelengths of 491 nm to excite MitoTracker Green (emission filtered at 525 nm) and 561 nm to excite **Gd.L2** (emission filtered at 620 nm). Images were captured by a highly sensitive 16-bit, 512 × 512 pixel back-illuminated EM-CCD camera (ImageEM 9100-13, Hamamatsu). Volocity software (PerkinElmer) provided the user interface.

In Vivo Tissue Isolation and Imaging. Islet isolation was carried out as shown in ref 67. In short, a female CD1 mouse (8−12 weeks old) was sacrificed by cervical dislocation. The pancreas was injected with 1 mg/mL collagenase solution through the bile duct and excised. The pancreas was digested by heating with collagenase solution, and islets were isolated through the use of ficoll gradient centrifugation. Islets were hand-picked and kept at 37 °C in Islet medium (RPMI supplemented with 10% FBS and 1% penicillin/streptomycin). Islets were dispersed into clusters and single cells according to the procedure in ref 67. Briefly, islets were incubated with Hank's based enzyme-free dissociation buffer (Invitrogen, Paisley, UK) and centrifuged. All but 1 mL of the supernatant was removed, and the pellet was resuspended vigorously via pipetting. The cells were washed and resuspended with RPMI 1640 and then loaded onto a poly-L-lysine-treated coverslip. On the day of visualization, cells were washed twice with KREBS buffer (140 mM NaCl, 3.6 mM KCl, 0.5 mM NaH_2PO_4, 0.2 mM $MgSO_4$, 1.5 mM $CaCl_2$, 10 mM HEPES, pH 7.4, 2 mM $NaHCO_3$) pre-equilibrated with 95:5 O_2/CO_2 and containing 25 mM glucose. Cells were then incubated with KREBS buffer containing 215 mM **Gd.L2** and 100 nM MitoTracker Green for 30 min and washed twice with KREBS buffer before visualization. Images were captured using a Zeiss Axiovert confocal microscope coupled to a Nipkow spinning-disk head (Yokogawa CSU-10) using a 63× oil objective. A solid-state laser (CrystaLaser) controlled by a laser-merge module (Spectral Applied Physics) provided wavelengths of 491 nm to excite MitoTracker Green

dx.doi.org/10.1021/ic402233g | Inorg. Chem. 2013, 52, 14284−14293

(emission filtered at 525 nm) and 561 nm to excite **Gd.L2** (emission filtered at 620 nm). Images were captured by a highly sensitive 16-bit, 512 × 512 pixel back-illuminated EM-CCD camera (ImageEM 9100-13, Hamamatsu). Volocity software (PerkinElmer) provided the user interface.

Synthesis of 3. DO3A-*t*-Bu-ester (0.16 g, 0.28 mmol) and K_2CO_3 (0.05 g, 0.34 mmol) were dissolved in MeCN (5 mL), and the mixture was stirred for 5 min. **2** (0.15 g, 0.28 mmol) in MeCN (15 mL) was added dropwise. The reaction mixture was heated to reflux temperatures for 24 h. The resulting solution was filtered, and the filtrate was concentrated under reduced pressure. The crude product was purified by silica gel chromatography with 1−20% MeOH/DCM, 1% NH_3 solution (28%), affording **3** as a beige solid (0.21 g, 37%). ^{1}H NMR (400 MHz, $CDCl_3$): δ 1.18 (t, 12H, $^3J_{HH}$ = 7.1 Hz), 1.43 (s, 27 H), 2.09−2.15 (m, 2H), 2.29−3.06 (m, 16H), 3.13−3.19 (m, 2H), 3.36 (q, 8H, $^3J_{HH}$ = 7.4 Hz), 3.50 (s, 6H), 6.23−6.43 (m, 6H), 7.04−7.08 (m, 1H), 7.41−7.47 (m, 2H), 7.81−7.84 (m, 1H). ^{13}C NMR (100 MHz, $CDCl_3$): δ 12.6, 28.0, 30.9, 36.0, 44.3, 46.2, 49.6, 51.0, 53.5, 55.8, 56.4, 65.2, 82.0, 82.4, 97.9, 105.1, 107.8, 122.6, 123.8, 128.0, 128.7, 131.0, 132.4, 148.8, 153.4, 153.5, 168.4, 172.5. ESI-HRMS: calcd for $C_{56}H_{83}N_7O_8$ 982.6381, found *m*/*z* 982.6398.

Synthesis of L1. **3** (0.20 g, 1 mmol) was dissolved in CH_2Cl_2 (2 mL), and trifluoroacetic acid (2 mL) was added dropwise. The solution was stirred at room temperature, open to air, for 24 h. The solvents were removed in vacuo, and the residue was redissolved in CH_2Cl_2. This was repeated with diethyl ether and again with CH_2Cl_2 until **L1** was obtained as a bright-pink solid (0.16 g, 96%). ^{1}H NMR (400 MHz, $CDCl_3$): δ 1.17 (t, 12H, $^3J_{HH}$ = 7.2 Hz), 3.06−3.71 (m, 24H), 4.20 (m, 2H), 6.54−6.75 (m, 6H), 7.14 (d, 1H), 7.60−7.64 (m, 2H), 7.80 (d, 1H). ^{13}C NMR (100 MHz, $CDCl_3$): δ 11.06, 34.14, 45.42, 45.63, 48.18, 49.33, 51.97, 52.26, 54.41, 110.36, 122.90, 124.22, 126.14, 128.62, 128.82, 129.83, 133.57, 153.00, 153.35, 160.78, 169.12. ESI-HRMS: calcd for $C_{44}H_{60}N_7O_8$ 814.4503, found *m*/*z* 814.4503.

Synthesis of Gd.L1. **L1** (0.04 g, 0.05 mmol) and $GdCl_3{\cdot}6H_2O$ (0.01 g, 0.03 mmol) were dissolved in water (2 mL), and the pH was adjusted to 5.5 using 1 M NaOH solution. The mixture was stirred at room temperature for 24 h. The reaction precipitate was filtered and then dissolved in DCM. The organic layer was washed with water and then dried over $MgSO_4$. Addition of ether to this solution precipitated **Gd.L1** as a pale-beige powder (0.022 g, 84%). ESI-HRMS: calcd for $C_{44}H_{57}N_7O_8Gd$ 969.3510, found *m*/*z* 969.3569.

Synthesis of Tb.L1. The complex was prepared by an method analogous to that for **Gd.L1** using **L1** (0.26 g, 0.32 mmol) and $TbCl_3{\cdot}6H_2O$ (0.06 g, 0.16 mmol) to yield **Tb.L1** as a pale-beige solid (0.12 g, 80%). ESI-HRMS: calcd for $C_{44}H_{57}N_7O_8Tb$ 970.3522, found *m*/*z* 970.3555.

Synthesis of 5. **4** (0.50 g, 1.03 mmol) was dissolved in DCM (10 mL), and NEt_3 (0.1 mL, 1.24 mmol) was added. The reaction mixture was cooled to 0 °C using an ice bath, and chloroacetyl chloride (0.1 mL, 1.24 mmol) in DCM (5 mL) was then added dropwise. The reaction mixture was allowed to come to room temperature. The solution was stirred at room temperature for 5 h, and then the solvent was removed under reduced pressure. The resultant solid was dissolved in DCM (20 mL) and washed with water (10 mL × 2) and brine. The organic extract was dried over $MgSO_4$ and evaporated to give **5** as a purple solid (0.36 g, 62%). ^{1}H NMR (400 MHz, $CDCl_3$): δ 1.18 (t, 12H, $^3J_{HH}$ = 7.0 Hz), 3.10 (t, 2H, $^3J_{HH}$ = 7.1 Hz), 3.34 (q, 10H, $^3J_{HH}$ = 7.2 Hz), 3.95 (s, 2H), 6.31−6.47 (m, 6H), 7.08−7.11 (m, 1H), 7.46−7.48 (m, 2H), 7.93−7.96 (m, 1H). ^{13}C NMR (100 MHz, $CDCl_3$): δ 12.42, 39.50, 40.39, 41.43, 42.42, 45.01, 65.65, 98.87, 108.96, 123.08, 123.88, 128.41, 128.53, 130.22, 133.03, 148.26, 153.17, 153.55, 166.80, 169.46, 169.85. ESI-HRMS: calcd for $C_{32}H_{38}ClN_4O_3$ 561.2632, found *m*/*z* 561.2646.

Synthesis of 6. Tri-*tert*-butyl-DO3A (0.32 g, 0.59 mmol) and K_2CO_3 (0.08 g, 0.59 mmol) were dissolved in MeCN (20 mL) and left to stir for 5 min. **5** in MeCN (20 mL) was then added dropwise. The reaction mixture was heated to reflux for 24 h. The resulting solution was filtered, and the filtrate was concentrated under reduced pressure. The crude product was purified by silica gel chromatography using 1−20% MeOH/DCM, 1% NH_3 solution (33%), affording **6** as a beige solid (0.12 g, 21%). ^{1}H NMR (400 MHz, $CDCl_3$): δ 1.18 (t, 12H, $^3J_{HH}$ = 7.0 Hz), 1.40 (s, 27H), 1.98−2.92 (m, 28H), 3.28 (q, 8H, $^3J_{HH}$ = 7.1 Hz), 6.24−6.41 (m, 6H), 7.01−7.04 (m, 1H), 7.35−7.45 (m, 2H), 7.76−7.83 (m, 1H). ^{13}C NMR (100 MHz, $CDCl_3$): δ 12.53, 27.86, 30.94, 40.00, 40.55, 44.31, 49.01, 50.27, 51.13, 55.66, 56.22, 65.43, 81.52, 97.68, 104.84, 108.17, 122.73, 123.84, 128.38, 130.05, 132.84, 148.8, 153.18, 169.63, 170.58, 171.01, 172.31. ESI-HRMS: calcd for $C_{58}H_{87}N_8O_9$ 1039.6596, found *m*/*z* 1039.6676.

Synthesis of L2. **6** (0.30 g, 0.3 mmol) was stirred in CH_2Cl_2 (1 mL), and trifluoroacetic acid (1 mL, excess) was added dropwise. The solution was stirred at room temperature, open to air, for 24 h. The solvents were then removed in vacuo, and the residue was redissolved in CH_2Cl_2. This was again removed, and diethyl ether was added. After removal of diethyl ether, this process was repeated, affording **L2** as a pink solid (0.23 g, 92%). ^{1}H NMR (400 MHz, MeOD): δ 1.15 (t, 12H, $^3J_{HH}$ = 6.0 Hz), 2.84 (t, 2H, $^3J_{HH}$ = 7.0 Hz), 2.97−3.95 (m, 26H), 3.54 (q, 8H, $^3J_{HH}$ = 6.0 Hz), 6.60−6.66 (m, 6H), 7.11 (d, 1H), 7.59 (m, 2H), 7.90 (d, 1H). ^{13}C NMR (100 MHz, $CDCl_3$): δ 10.88, 38.29, 39.01, 45.44, 46.52, 50.41, 53.10, 110.98, 115.25, 122.42, 123.66, 128.55, 128.91, 133.06, 153.05, 161.17, 161.51, 169.20. ESI-HRMS: calcd for $C_{46}H_{63}N_8O_9$ 871.4702, found *m*/*z* 871.4718.

Synthesis of Gd.L2. **L2** (0.19 g, 0.22 mmol) and $GdCl_3{\cdot}6H_2O$ (0.04 g, 0.11 mmol) were dissolved in water (2 mL), and the pH was adjusted to 5.5 using 1 M NaOH(aq). The reaction was left stirring at room temperature overnight. The solution was removed in vacuo until a small volume was left. This crude solution was purified using Sephadex G10 chromotography, affording **Gd.L2** as a pale-beige solid (0.03 g, 27%). ESI-HRMS: calcd for $C_{46}H_{60}GdN_8O_9$ 1026.3724, found *m*/*z* 1026.3834.

Synthesis of Tb.L2. The complex was prepared by an method analogous to that for **Gd.L2** using **L2** (0.19 g, 0.21 mmol) and $TbCl_3{\cdot}6H_2O$ (0.04 g, 0.11 mmol) to yield **Tb.L2** as a pale-beige solid (0.03 g, 27%). ESI-HRMS (MeOH): calcd for $C_{46}H_{60}N_8O_9Tb$ 1027.3737, found *m*/*z* 1027.3805.

■ ASSOCIATED CONTENT

Ⓢ Supporting Information

Luminescence decay data for **Tb.L1** and **Tb.L2**. This material is available free of charge via the Internet at http://pubs.acs.org.

■ AUTHOR INFORMATION

Corresponding Author

*E-mail: n.long@imperial.ac.uk.

Notes

The authors declare no competing financial interest.

■ ACKNOWLEDGMENTS

N.J.L. and G.A.R. were supported by a grant from the Wellcome Trust Institutional Strategic Support Fund. G.A.R. was supported by Wellcome Trust Senior Investigator (WT098424AIA), MRC Programme (MR/J0003042/1), and Diabetes UK Project (11/0004210) grants and is the recipient of a Royal Society Wolfson Research Merit Award. The work leading to this publication received support from the Innovative Medicines Initiative Joint Undertaking under Grant Agreement 155005 (IMIDIA), resources of which are composed of financial contributions from the European Union's Seventh Framework Programme (FP7/2007-2013) and EFPIA companies' in-kind contribution (G.A.R.). We also thank Imperial College London for funding, Dr. Pauline Chabosseau (Cell Biology) for kind assistance with single cell imaging, Dr. Israt Alam (Surgery and Cancer) for assistance with mice work, and Dr. Ioannis Lavdas (Surgery and Cancer) for MRI coil setup and expertise.

REFERENCES

(1) Aime, S.; Crich, S. G.; Gianolino, E.; Giovenzana, G. B.; Tei, L.; Terreno, E. *Coord. Chem. Rev.* **2006**, *250*, 1562−1579.
(2) Tóth, É.; Helm, L.; Merbach, A. E. *Top. Curr. Chem.* **2002**, *221*, 61−101.
(3) Frullano, L.; Meade, T. J. *J. Biol. Inorg. Chem.* **2007**, *12*, 939−949.
(4) Bünzli, J.-C. G.; Piguet, C. *Chem. Soc. Rev.* **2005**, *34*, 1048−1077.
(5) Montgomery, C. P.; Murray, B. S.; New, E. J.; Pal, R.; Parker, D. *Acc. Chem. Res.* **2009**, *42*, 925−937.
(6) Faulkner, S.; Burton-Pye, B. P.; Pope, S. J. A. *Appl. Spectrosc. Rev.* **2005**, *40*, 1−39.
(7) Manella, C. *Biochim. Biophys. Acta* **2006**, *1762*, 140−147.
(8) David, S.; Weiss, M. J.; Wong, J. R.; Lampidis, T. J.; Chen, L. B. *J. Biol. Chem.* **1985**, *260*, 13844−13850.
(9) Dairkee, S. H.; Hackett, A. J. *Breast Cancer Res. Treat.* **1991**, *18*, 57−61.
(10) Duchen, M. R. *Mol. Aspects Med.* **2004**, *25*, 365−451.
(11) Caravan, P.; Ellison, J. J.; McMurry, T. J.; Lauffer, R. B. *Chem. Rev.* **1999**, *99*, 2293−2352.
(12) Caravan, P. *Chem. Soc. Rev.* **2006**, *35*, 512−523.
(13) Weissleder, R.; Ross, B.; Rehemtulla, A.; Gambhir, S. *Molecular Imaging: Principles and Practice*; PMPH-USA: Shelton, CT, 2010.
(14) Comblin, V.; Gilsoul, D.; Hermann, M.; Humblet, V.; Jacques, V.; Mesbahi, M.; Sauvage, C.; Desreux, J. *Coord. Chem. Rev.* **1999**, *185*, 451−470.
(15) Esqueda, A. C.; López, J. A.; Andreu-de-Riquer, G.; Alvarado-Monzón, J. C.; Ratnaker, J.; Lubag, A. J. M.; Sherry, A. D.; De León-Rodríguez, L. M. *J. Am. Chem. Soc.* **2009**, *131*, 11387−11391.
(16) Polasek, M.; Caravan, P. *Inorg. Chem.* **2013**, *52*, 4084−4096.
(17) Reguerio-Figueroa, M.; Bensenane, B.; Ruscsák, E.; Esteban-Gómez, D.; Charbonnière, L. J.; Tircsó, G.; Tóth, I.; de Blas, A.; Rodríguez-Blas, T.; Platas-Iglesias, C. *Inorg. Chem.* **2011**, *50*, 4125−4141.
(18) Placidi, M. P.; Engelmann, J.; Natarajan, L. S.; Logothetis, N. K.; Angelovski, G. *Chem. Commun.* **2011**, *47*, 11534−11536.
(19) Faulkner, S.; Pope, S. J. A.; Burton-Pye, B. P. *Appl. Spectrosc. Rev.* **2005**, *40*, 1−39.
(20) Parker, D.; Dickins, R. S.; Puschmann, H.; Crossland, C.; Howard, J. A. K. *Chem. Rev.* **2002**, *102*, 1977−2010.
(21) Murray, B. S.; New, E. J.; Pal, R.; Parker, D. *Org. Biomol. Chem.* **2008**, *6*, 2085−2094.
(22) Atkins, P.; de Paula, J. *Physical Chemistry*, 8th ed.; Oxford University Press: Oxford, U.K., 2006.
(23) Bünzli, J.-C. G. *Acc. Chem. Res.* **2006**, *39*, 53−61.
(24) Gonçalves, M. S. T. *Chem. Rev.* **2009**, *109*, 190−212.
(25) Yuan, L.; Lin, W.; Zheng, K.; He, L.; Huang, W. *Chem. Soc. Rev.* **2013**, *42*, 622−661.
(26) Suksai, C.; Tuntulani, T. *Chem. Soc. Rev.* **2003**, *32*, 192−202.
(27) Bandichlov, R.; Petrescu, A. D.; Vespa, A.; Kier, A. B.; Schroeder, F.; Burgess, K. *Bioconjugate Chem.* **2006**, *17*, 1219−1225.
(28) Zhou, Y.; Kim, Y.-S.; Yan, X.; Jacobson, O.; Chen, X.; Liu, S. *Mol. Pharmaceutics* **2011**, *8*, 1198−1209.
(29) You, Y.; Tomat, E.; Hwang, K.; Atanasijevic, T.; Nam, W.; Jasanoff, A. P.; Lippard, S. J. *Chem. Commun.* **2010**, *46*, 4139−4141.
(30) Scadutro, R. C., Jr.; Grotyohann, L. W. *Biophys. J.* **1999**, *76*, 469−477.
(31) Longmuir, M. R.; Ogawa, M.; Hana, Y.; Kosaka, N.; Regino, C. A. S.; Choyke, P. L.; Kobayashi, H. *Bioconjugate Chem.* **2008**, *19*, 1735−1742.
(32) Lavis, L. D.; Chao, T.-Y.; Raines, R. T. *ACS Chem. Biol.* **2006**, *1*, 252−260.
(33) Hockings, P. D.; Rogers, P. J. *Biochim. Biophys. Acta* **1996**, *1282*, 101−106.
(34) Huang, S. G. *J. Biomol. Screening* **2002**, *7*, 383−389.
(35) Lefevre, C.; Kang, H. C.; Haugland, R. P.; Malakzadeh, N.; Arttamangkul, S.; Haugland, R. P. *Bioconjugate Chem.* **1996**, *7*, 482−489.
(36) Chen, X.; Pradhan, T.; Wang, F.; Kim, J. S.; Yoon, J. *Chem. Rev.* **2012**, *112*, 1910−1956.
(37) Best, Q. A.; Xu, R.; McCarroll, M. E.; Wang, L.; Dyer, D. J. *Org. Lett.* **2010**, *12*, 3219−3221.
(38) Lee, M. H.; Han, J. H.; Lee, J. H.; Park, N.; Kumar, R.; Kang, C.; Kim, J. S. *Angew. Chem., Int. Ed.* **2013**, *52*, 6206−6209.
(39) Jennings, L. E.; Long, N. J. *Chem. Commun.* **2009**, 3511−3524.
(40) Stasiuk, G. J.; Long, N. J. *Chem. Commun.* **2013**, *49*, 2732−2746.
(41) Guo, K.; Berezin, M. Y.; Zheng, J.; Akers, W.; Lin, F.; Teng, B.; Vasalatiy, O.; Gandjbakhche, A.; Griffiths, G. L.; Achilefu, S. *Chem. Commun.* **2010**, *46*, 3705−3707.
(42) Hao, D.; Ai, T.; Goerner, F.; Hu, X.; Runge, V. M.; Tweedle, M. *J. Magn. Reson. Imaging* **2012**, *36*, 1060−1071.
(43) Hüber, M. M.; Staubli, A. B.; Kustedjo, K.; Gray, M. H. B.; Shih, J.; Fraser, S. E.; Jacobs, R. E.; Meade, T. J. *Bioconjugate Chem.* **1998**, *9*, 242−249.
(44) Yamane, T.; Hanaoka, K.; Muramatsu, Y.; Tamura, K.; Adachi, Y.; Miyashita, Y.; Hirata, Y.; Nagano, T. *Bioconjugate Chem.* **2011**, *22*, 2227−2236.
(45) Yan, X.; Zhou, Y.; Liu, S. *Theranostics* **2012**, *2*, 988−998.
(46) Barge, A.; Cravotto, G.; Gianolio, E.; Fedeli, F. *Contrast Med. Mol. Imaging* **2006**, *1*, 184−188.
(47) Beija, M.; Afonso, C. A. M.; Martinho, J. M. G. *Chem. Soc. Rev.* **2009**, *38*, 2410−2433.
(48) Beeby, A.; Clarkson, I. M.; Dickins, R. S.; Faulkner, S.; Parker, D.; Royle, L.; de Sousa, A. S.; Williams, J. A. G.; Woods, M. *J. Chem. Soc., Perkin Trans. 2* **1999**, 493−503.
(49) Bruce, J. A.; Lowe, M. P.; Parker, D. *Photophysiscal Aspects of Lanthanide(III) Complexes: The Chemistry of Contrast Agents in Medical Magnetic Resonance Imaging*; Wiley; West Sussex, U.K., 2001.
(50) Horrocks, W. D.; Sudnick, D. R. *J. Am. Chem. Soc.* **1979**, *101*, 334−340.
(51) Fasano, M.; Curry, S.; Terreno, E.; Galliano, M.; Fanali, G.; Narciso, P.; Notari, S.; Ascenzi, P. *IUBMB Life* **2005**, *57*, 787−796.
(52) Boros, E.; Caravan, P. *J. Med. Chem.* **2013**, *56*, 1782−1786.
(53) Cai, H.-H.; Zhong, X.; Yang, P.-H.; Wei, W.; Chen, J.; Cai, J. *Colloids Surf., A* **2010**, *372*, 35−40.
(54) Caravan, P. *Acc. Chem. Res.* **2009**, *42*, 851−862.
(55) Caravan, P.; Zhang, Z. *Eur. J. Inorg. Chem.* **2012**, 1916−1923.
(56) Estrella, V.; Chen, T.; Lloyd, M.; Wotjkowiak, J.; Cornnell, H. H.; Ibrahim-Hashim, A.; Bailey, K.; Balagurunathan, Y.; Rothberg, J. M.; Sloane, B. F.; Johnson, J.; Gatenby, R. A.; Gillies, R. J. *Cancer Res.* **2013**, *73*, 1524−1535.
(57) Zhao, Z.; Chan, P.-S.; Li, H.; Wong, K.-L.; Wong, R. N. S.; Mak, N.-K.; Zhang, J.; Tam, H.-L.; Wong, W.-Y.; Kwong, D. W. J.; Wong, W.-K. *Inorg. Chem.* **2012**, *51*, 812−821.
(58) Reungpatthanaphong, P.; Dechsupa, S.; Meesungnoen, J.; Loetchutinat, C.; Mankhetkorn, S. *J. Biochem. Biophys. Methods* **2003**, *57*, 1−16.
(59) Shiraishi, Y.; Sumiya, S.; Kohno, Y.; Hirai, T. *J. Org. Chem.* **2008**, *73*, 8571−8574.
(60) Zhang, X.; Shiraishi, Y.; Hirai, T. *Org. Lett.* **2007**, *9*, 5039−5042.
(61) Zheng, Y.; Yang, Z.; Ying, J. Y. *Adv. Mater.* **2007**, *19*, 1475−1479.
(62) Chauvin, A.-S.; Gumy, F.; Imbert, D.; Bünzli, J.-C. G. *Spectrosc. Lett.* **2004**, *37*, 517−532.
(63) Corsi, D. M.; Platas-Iglesias, C.; van Bekum, H.; Peters, J. A. *Magn. Reson. Chem.* **2001**, *39*, 723−726.
(64) Workman, P.; Aboagye, E. O.; Balkwill, F.; Balmain, A.; Bruder, G.; Chaplin, D. J.; Double, J. A.; Everitt, J.; Farningham, D. A. H.; Glennie, M. J.; Kelland, L. R.; Robinson, V.; Stratford, I. J.; Tozer, G. M.; Watson, S.; Wedge, S. R.; Eccles, S. A. *Br. J. Cancer* **2010**, *102*, 1555−1577.
(65) Lavdas, I.; Seton, H. C.; Harrington, C. R.; Wischik, C. M. *Magn. Reson. Mater. Phys.* **2011**, *24*, 331−337.
(66) Rasband, W. S. *ImageJ*; U.S. National Institutes of Health: Bethesda, MD, 1997−2012; http://rsb.info.nih.gov/ij/.
(67) Ravier, M. A.; Rutter, G. A. *Methods Mol. Biol.* **2010**, *633*, 171−184.